Shelf slope convection: A note for Antarctic regions(*)

S. PIACSEK(^{1}), M. POTTS(^{2}), L. CASTELLANA(^{3}) and R. PURINI(^{3})

(^{1}) *Naval Research Laboratory, Stennis Space Center - MS, USA*
(^{2}) *Krispin Technologies - Rockville, MD, USA*
(^{3}) *Istituto Talassografico, CNR - Trieste, Italy*

Summary. — Some basic processes associated with buoyancy-driven convection in the presence of coastal upwelling currents were investigated in a 2.5D framework near the Adelie Coast of Antarctica. The surface buoyancy forcing was derived from cooling and brine deposition due to ice formation, and was specified over a persistent off-shore polynya maintained by the off-shore katabatic winds. Rotational effects and the formation of a turbulent surface mixed layer were included in the model. The representation of topography was done via the VBM (virtual Boundary Method) that utilizes equivalent body forces in the momentum equation, thus enabling the use of very efficient Poisson solvers for the pressure, based on FFTs. The simulations were carried out near longitude 143E, between latitude 68S and 65S, over the near-shore shelf region. The hydrography was initialized with the 1/4 deg Levitus annual climatology. Two cases of idealized meteorological forcing were considered: constant winds blowing along-shore and off-shore. The resultant motions in each case were characterized by interaction between the wind-driven upwelling motions and the downward moving dense convection plumes, but with marked differences: a) the formation of a strong front under the open sea edge of the polynya only by off-shore winds; b) the periodic suppression of the surface off-shore currents and of the coastal upwelling only by the along-shore winds; c) the formation of deep upwelling currents along the slope between 400 and 200 meters only for along-shore winds, and d) the rapid filling of the surface layers (depths < 100 m) with high salinities under the whole polynya by the off-shore forcing, *vs.* the delayed filling of a narrow region near the downwelling plume with intermediate salinity values by the along-shore forcing.

PACS 92.10.-c – Physics of the oceans.
PACS 93.30.Sq – Polar regions.
PACS 02.60.Cb – Numerical simulation; solution of equations.

1. – Introduction

The processes by which deep and bottom waters form in the world ocean are of crucial importance to the whole Earth's climate. It is mostly the dense deep and bottom waters that drive the meridional thermohaline conveyor belt circulation, which controls the redistribution of cold waters from high latitudes to the equatorial oceans, and of warm equatorial waters back up to the high latitudes (Broecker, 1991). In general, the sites of the world's deep and bottom water (DW, BW) formation are found in the high latitudes, in seas adjacent to the Arctic and the Antarctic (Rudels and Quadfasel, 1991; Foster and Carmack, 1976). Any strong warming and/or fresh water addition in these polar regions can lead to a decrease or even cessation of DW and BW formation, and hence to a decreased meridional heat transport. In light of the widely anticipated global warming, due in large part to the anthropogenic increase in atmospheric CO_2 levels, there is a need to better understand the processes involved in influencing the ocean component of the climate system (Broecker, 1997; Washington and Meehl, 1996).

DW and BW production occurs in both the deep open stretches and in the shelf regions of ocean basins. The former type of dense water formation is known as open ocean deep convection, whereas the latter is referred to as topographically influenced shelf convection. Examples of open ocean deep convection occur in the Greenland and Labrador Seas in the nordic seas, and in the Weddell and Ross Seas in the southern hemisphere. Shelf convection is usually very strong along the continental shelves of the Arctic Ocean and the Antarctic. The Antarctic and the North Atlantic contribute roughly equal amounts of dense water to the thermohaline circulation, which is thought to be a total of 25 Sverdrups.

While open ocean deep convection has been the subject of many observations and modeling efforts (Schlosser et al., 1991; Schott et al., 1993; Killworth, 1983; Marshall and Schott, 1998), the process of coastal dense water formation has undergone much fewer observational and simulation studies (Bindoff et al., 1997; Jacobs and Comiso, 1989; Kampf and Backhaus, 1998). This may be partly due to the fact that open ocean deep convection transports dense waters directly to considerable depths (down to 2000 m in the Greenland Sea!), whereas dense waters produced on shelves must descend the shelf slope in plumes undergoing complicated entrainment and topographic interaction processes.

1‘1. *Dense water formation and polynyas.* – Although not clearly understood, in polar regions dense water formation is associated, in wintertime, with the presence of large opening in the sea ice cover, named polynyas (Smith et al., 1990; Muench et al., 1995; Schneider and Budeus, 1995). Several polynyas affect the dynamic and thermodynamic processes on the Antarctic continental shelf, in particular the one found in Terra Nova Bay in the Ross Sea, where the concomitant presence of strong katabatic winds and the Drygalski Ice Tongue causes such a polynya to cover an area of about $1000 \, km^2$. It is necessary to point out that topographic variations play an important role in defining the extension and evolution of these ice-free ocean features.

Coastal polynyas are a perennial and extremely frequent occurrence in the waters surrounding the Antarctic continent. Although polynyas are usually categorized as either being caused by latent heat loss or sensible heat loss, many of the polynyas around Antarctica are thought to be hybrids (Jacobs and Comiso, 1989). A sensible heat component is supplied by upwelling of warm water; in particular, the Circumpolar Deep Water (CDW) provides a heat flux which partly balances the heat loss to the atmosphere (Ja-

cobs, 1989). A latent heat component is contributed by strong offshore katabatic winds that drive ice away from shore at the same time that they induce ice formation in the open water left behind the advected ice (Pease, 1987). The heat loss at these polynyas can be as high $1000\,W/m^2$, and can clearly lead to very vigorous ice production and brine rejection, resulting in strong thermohaline convection in the water column.

While much of the Antarctic Bottom Water (AABW) is thought to be produced in the Weddell Sea, Bindoff *et al.* (1997) suggest that a quarter of the AABW may be formed along the Adelie Coast. The Adelie Coast, like much of the Antarctic coast, is characterized by shallow (hundreds of meters deep) shelves that stretch for up to 100 kilometers or more offshore, followed by precipitous shelf breaks where the ocean depth may plunge to more than 4000 meters in depth within a few tens of kilometers. The Adelie depression found along the coast has no outlet to the open ocean other than over its sill of about 450 meters, and lends an extra complication since it can trap cold salty water that is formed along the surrounding shelves, rather than allowing break to the abyss. The depression area is also the site of the recurring Mertz Glacier Polynya which is situated generally over the depression itself and has been theorized to be the cause of much of the AABW formed along the Adelie Coast (Rintoul, 1997).

Smaller areas of ice-free oceans are called leads, and represent an opening in the ice cover caused by divergent ice motions. Because of their small areas, they only contribute appreciably to large-scale dense water formation if the cumulative exposed ocean area is large (typically thousands of km^2).

1˙2. *Nonhydrostatic oceanic motions.* – The hydrostatic approximation, in which vertical pressure gradients are balanced only by the local weight of the fluid, is generally appropriate for use in most ocean models. This is due to the large aspect ratio of horizontal to vertical length scales in most ocean basins (*e.g.*, 1000 km *vs.* 2 km), resulting in small vertical velocities and accelerations as determined by the mass continuity equation. Typical vertical velocities associated with large-scale oceanic flows are of the order of mm/s, *vs.* horizontal velocities ranging up to $\sim 1\,m/s$. However, under certain atmospheric or topographic forcing conditions the evolving motions develop horizontal to vertical length scale ratios between 1 and 10, and under these conditions the hydrostatic approximation begins to lose its validity. In certain regions of the Greenland Sea, for example, vertical velocities exceeding 5 cm/s have been measured by moored vertical ADCPs (Schott *et al.*, 1993).

Jones and Marshall (1993) have shown that open ocean deep convection, resulting from strong local buoyancy surface forcing, is an inherently nonhydrostatic process. This also appears to be the case for convection occurring in shallow waters on or near continental shelves, based on ongoing modeling and observational studies. In localized areas where strong convective cooling is combined with sharp changes in topography, such as those along the Antarctic coastal polynyas, the combined forcing can lead to dramatic vertical accelerations that are the trademark of nonhydrostatic events.

There have been several modeling studies for convection under leads (Smith and Morison, 1998; Muench *et al.*, 1995), but few for large polynyas. One reason for that is the much greater demand on computational resources needed to resolve the downwelling plumes and yet cover the large areas, even in 2D simulations.

1˙3. *Nonhydrostatic models with topography.* – Gawarkiewicz and Chapman (1995) have simulated the dense water formation on a shallow continental shelf with a 3D hydrostatic model, for a constant slope of 0.001. Because of the difficulty in introducing

topography into a nonhydrostatic model, none has yet been applied to the continental shelves. The main reason has been the lack of an efficient solver for the Poisson equation for pressure which is a component of all fully nonhydrostatic ocean models (*e.g.*, solvers based on FFTs could not be applied directly). One of the thrusts of this paper is the introduction and validation of a new technique to incorporate topography into a nonhydrostatic model, with slopes up to 0.01. A second thrust is the evaluation of the usefulness of this technique in an application to convection on a section of the Antarctic shelf.

The technique, known as the Virtual Boundary Method (VBM), imposes virtual topography inside a rectangular domain and utilizes equivalent body forces in the momentum equation. This allows the Poisson equation for pressure to be solved in an efficient manner (using FFTs) in either two or three dimensions. The VBM was first used by Goldstein *et al.* (1993, 1995) to model ridges along the edge of a boundary in a simulation of turbulent channel flow. This technique utilizes equivalent body forces in the momentum equation to represent the effects of topography. As a result, the Poisson equation for pressure could be solved with a very efficient method based on FFTs.

The present paper is one of the first few applications of this technique to a geophysical situation. Because of its novelty, it was subjected to some fairly rigorous testing in Potts (1998) through a comparison to direct 2D simulations with stepped topography using relaxation solvers (Piacsek and Toomre, 1980; Piacsek *et al.*, 1997).

Section **2** describes the model details, the forcing and the initial setup for the simulation of convection along the Antarctic shelf. The results and conclusions are presented in sects. **3** and **4**.

2. – Physical and model setting

The model was forced with surface buoyancy forcing represented by strong cooling and brine deposition due to ice formation. This forcing was applied over an off-shore polynya which is assumed to persist during the simulation time, presumably due to off-shore katabatic winds. Rotational effects and the formation of a turbulent surface mixed layer are included via the Kantha-Clayson (1994) mixed layer model, an extension of the Mellor-Yamada–type turbulence closure models for geophysical flows (Mellor and Yamada, 1982).

2`1. *The model equations.* – Model details are given in Potts (1998). Here we recall that it is a two-dimensional (X-Z) nonhydrostatic model, using the rigid-lid approximation. The model solves the primitive equations using variable vertical mixing coefficients that are computed by the mixed layer model developed by Kantha and Clayson (1994). The equations solved in the problem are the Boussinesq incompressible equations of motion in a rotating reference frame which in tensorial form are

$$(1) \qquad \frac{\partial U_i}{\partial x_i} = 0,$$

$$(2) \quad \frac{\partial U_j}{\partial t} + \frac{\partial}{\partial x_k}(U_k U_j) + \varepsilon_{jkl} f_k U_l = -\frac{\partial P}{\partial x_j} - g\frac{\rho'}{\rho_0} + K_{\mathrm{mh}}\frac{\partial^2 U_j}{\partial x_\alpha \partial x_\alpha} + K_{\mathrm{mv}}\frac{\partial^2 U_j}{\partial x_3^2} + F_j(t),$$

$$(3) \qquad \frac{\partial \Theta}{\partial t} + \frac{\partial}{\partial x_k}(U_k \Theta) = K_{\mathrm{hh}}\frac{\partial^2 \Theta}{\partial x_\alpha \partial x_\alpha} + K_{\mathrm{hv}}\frac{\partial^2 \Theta}{\partial x_3^2},$$

$$(4) \qquad \frac{\partial S}{\partial t} + \frac{\partial}{\partial x_k}(U_k S) + K_{\mathrm{hh}}\frac{\partial^2 S}{\partial x_\alpha \partial x_\alpha} + K_{\mathrm{hv}}\frac{\partial^2 S}{\partial x_3^2}.$$

Equation (1) is the incompressible continuity equation and eq. (2) is the momentum equation in x, y, and z directions, with f_k being the k component of the rotation vector, g being the gravity and $\alpha = 1, 2$. The reference density is ρ, and ρ' is the deviation from the average density on a given horizontal section. To simulate topography, a body force has been added to the momentum equation in the form of $F_j(t)$, the computation of which is discussed in the next section.

For the two-dimensional case discussed in this paper, all variables are taken to be homogeneous in the y-direction, but the v velocity is nonzero as is appropriate when rotation is nonzero. Equations (3) and (4) represent conservation of potential temperature and salinity. The potential density and ρ are calculated using the UNESCO empirical equation of state. The mixing coefficients K_{mh}, K_{mv}, K_{hh}, and K_{hv} are the horizontal and vertical mixing coefficients for momentum and scalars. K_{mv} and K_{hv} are both computed by the second moment closure-based turbulent mixed layer model of Kantha and Clayson (1994), while the horizontal mixing coefficients K_{mh} and K_{hh} are taken to be constants.

This technique employs an external forcing function or body force that is computed at each time step. The body force is computed such that it forces flow along a particular surface within the flow field to be zero (the flow can be forced to other values as well if the no-slip condition is not desired) while at the same time maintaining continuity in the flow. This has the effect of simulating topography within the fluid, since the effect of topography is to bring fluid to rest at the bottom surface. The technique allows topography to be imposed within a rectangular domain without changing the solution technique of the pressure equation, and thus does not require major changes to the entire solution method.

The forcing function takes the form

$$(5) \qquad F_j(x_s, t) = \alpha \int_0^t U(x_s, t') \, \mathrm{d}t' + \beta U(x_s, t),$$

with

$$(6) \qquad F_i(x_s, t^n) = \left[\alpha \sum_{s=1}^{n} U_i^s \Delta t \right] + \beta U_i^n,$$

$$F_j(x_s, t^n) = \left[\alpha \sum_{s=1}^{n} V_i^s \Delta t \right] + \beta V_i^n,$$

$$F_k(x_s, t^n) = \left[\alpha \sum_{s=1}^{n} W_i^s \Delta t \right] + \beta W_i^n.$$

Echoing the previous study by Potts (1998), most of the simulations were carried out near longitude 143E, between latitude 68S and 65S, near the Adelie Coast of Antarctica). The extent of the polynya was from 400 m to 8 km off-shore, and the depth of the simulation volume was 400 m. The initial T, S profiles were made constant in latitude, with values corresponding to the mean of the region, and were slightly adjusted to make the initial density profile stable. Topography was taken from the ETOPO5 5 min data base. The hydrographic fields were extracted from the 1/4 degree annual mean Levitus climatology.

Two cases of idealized meteorological forcing were considered: along-shore and off-shore winds, with strengths of 1 dyne/cm^2 for each case. The direction of the along-

shore winds was eastward, so that the corresponding upwelling currents had an off-shore northerly component.

3. – Results and discussion

Figures 1–3 give a parallel illustration of the time evolution of the temperature field under off-shore (left columns) and along-shore (right columns) wind forcing. Figure 4 shows enlarged snapshots of the flow and temperature fields at $t = 10$ days for the two forcings. Figure 5 shows snapshots of the evolution of the salinity field for the two cases, and fig. 6 compares the salinity fields in the alongs-hore case for $t = 3$ days and $t = 12.5$ days.

Both wind forcings lead to competing development of the coastal upwelling currents and the downward moving convective plumes. However, there are striking differences for the two forcing cases, including the onset of convection, movement of the convection plumes, cessation of upwelling and flow reversals.

3˙1. *Initial evolution from* 1 *to* 2.5 *days.* – Figure 1 illustrates the development for this time period. Up to 24 hours there are only small differences. Both show the commencement of the coastal upwelling currents and the associated lifting of warmer and saltier waters up along the slope from below, but only the off-shore case shows the beginning of a convective downwelling near the edge of the polynya. By 36 hours the downwelling has developed into a strong, narrow downward plume, growing even more intense by 60 hours and forming what appears to be a front. In addition, the off-shore wind case has developed a second downwelling plume activity over the topographic trough located about 5 km from shore. Meanwhile, there is no sign of convection yet in the along-shore case.

3˙2. *Evolution from* 4 *to* 6 *days.* – The time evolution for this period is illustrated in fig. 2. The velocity patterns for the off-shore case remain the same, with upwelling motions continuing up-slope near the coast, while the frontal and center plumes remain in the same location, with little variation in intensity. The polynya edge front tends to confine the convective motions to the region between the front and the coast. It appears that the front funnels the recirculating motions of both the convection and upwelling back toward the shore and downward. As a result, the outflow from the bottom of the frontal plume feeds into the outflow from the downwelling center plume, and the combined effect of the accumulation of dense water in this region leads to the beginning of a sinking motion down the slope: by 6 days the dense plume has descended along the bottom below 400 m depth.

In the period 5 to 6 days even the along-shore case starts to develop convective activity, with a single plume descending about 2.5 km from shore. The ascending motions associated with this convective cell reinforce the wind-driven upwelling currents near the shore, leading to much stronger near-shore upward motions than in the off-shore case (see fig. 4 for enhanced details). It appears, however, that this strong recirculation may be the cause of a diminished accumulation of dense waters in the region below the plume, for at this time there is no evidence of any sinking motions along the bottom for the along-shore case.

3˙3. *Late evolution from* 6.5 *to* 10 *days.* – The overall evolution for this period is illustrated in fig. 3, with a special enlarged comparison in fig. 4 for the temperature at $t = 10$ days, and for the along-shore case salinities at $t = 3$ and 12.5 days, to illustrate
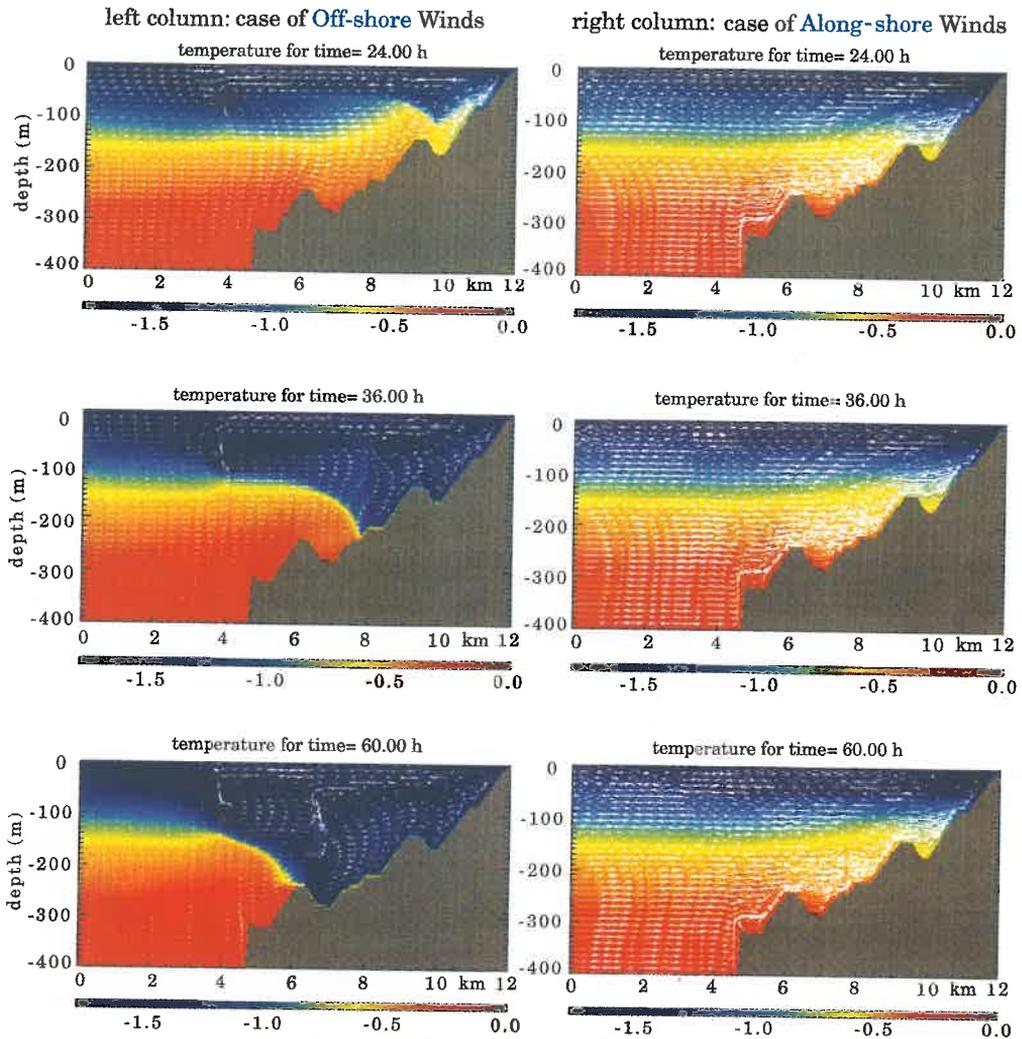
Fig. 1. – Time evolution of the temperature field from day 1 to day 2.5 for the two cases: a) left column, off-shore forcing; b) right column, along-shore forcing. The domain extent is 12 km off-shore and 400 m deep.

the great differences between the late stages of convection and upwelling for the two different wind forcing cases.

Again, there is little change in the upwelling and convective velocity patterns for the off-shore case, the only apparent change being the strong growth of the cold (dense) water region along the bottom, from a width of about 1 km at day 6.5 to a width of about 4 km by 10 days.

The along-shore case, meanwhile, has developed some strong variations, with the downward convective plume beginning to oscillate its location, from 2 km off-shore at day 6.5 to 3.5 km at day 7 and back to 1.5 km at day 10. At this latest time the downward plume has some indication of a double-plume structure. The most important effect of
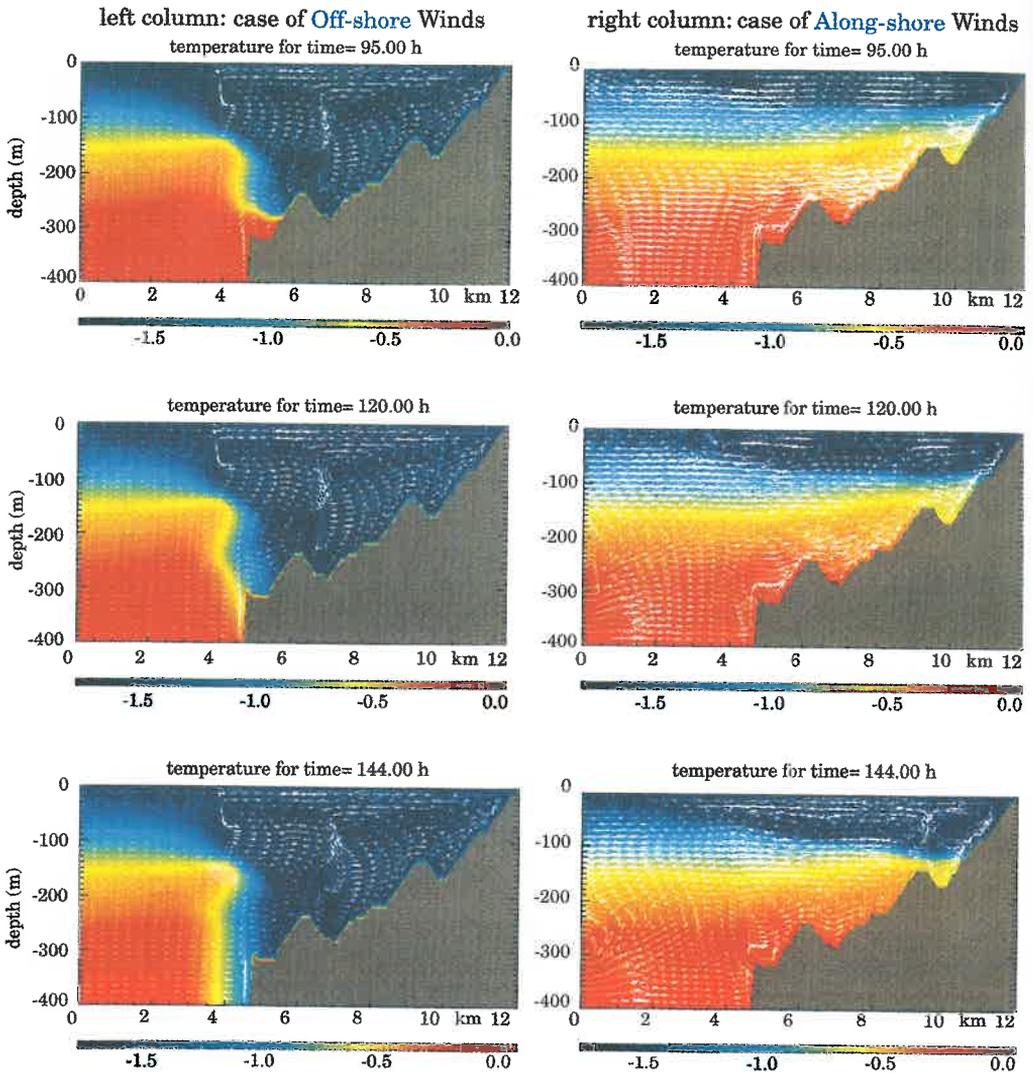
Fig. 2. – Time evolution of the temperature field from day 1 to day 2.5 for the two cases: a) left column, off-shore forcing; b) right column, along-shore forcing. The domain extent is 12 km off-shore and 400 m deep.

this location variation is the suppression of the upwelling movements near the coastal slope when the plume is about 1.5 km from shore. It is only at this time that dense water begins to accumulate over the ridge at 2.5 km from shore, and a downward flow develops along the bottom slope. Figure 4 for the along-shore case at $t = 12.5$ days illustrates this point better, and also the difference between the two cases. In the off-shore case the downward movement of the dense water was concentrated in a jet along the bottom, but in the along-shore case the flow of the heavy, cold water is both downward and away from shore, resulting in what appears to be a displacement of the warmer fluid volume over a broad area. In fact, the along-shore wind forced flow pattern at 10 days appears
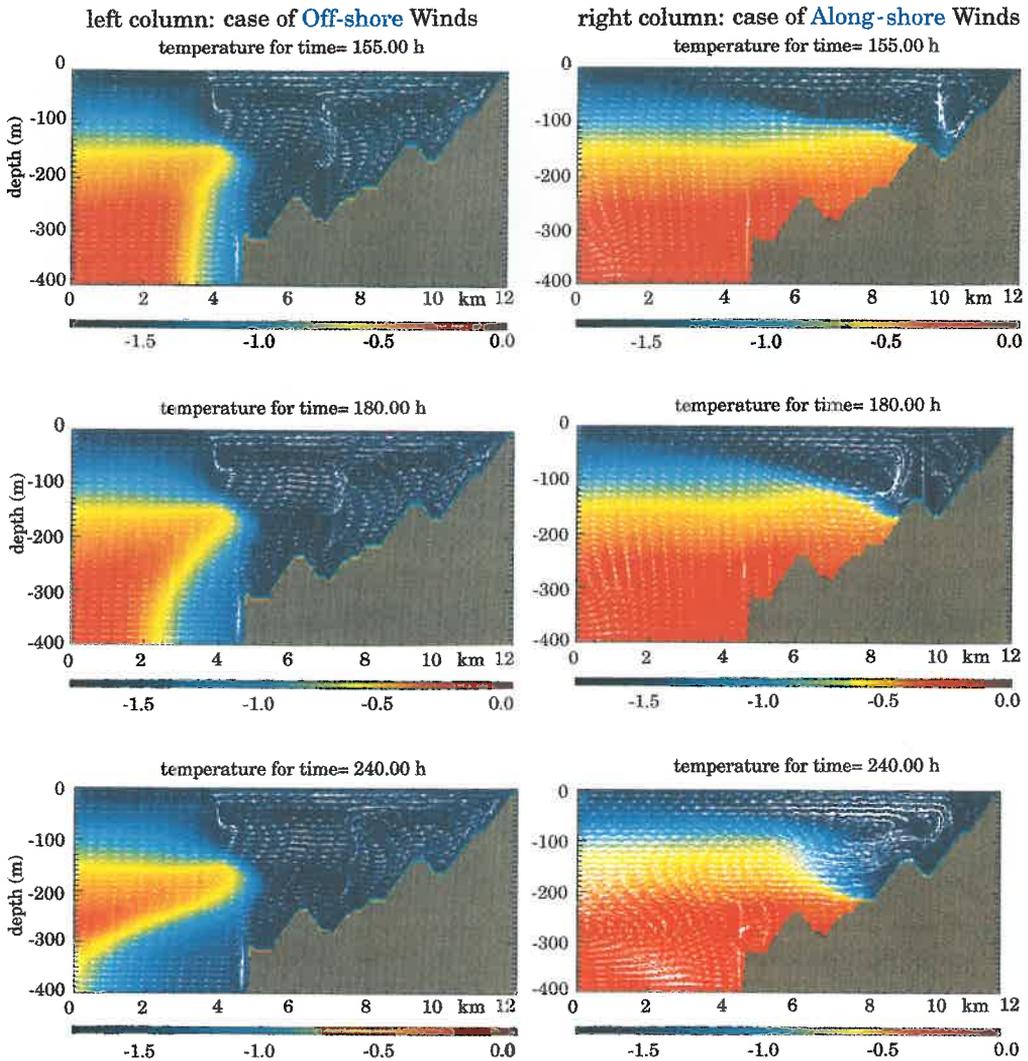
Fig. 3. – Time evolution of the temperature field from day 1 to day 2.5 for the two cases: a) left column, off-shore forcing; b) right column, along-shore forcing. The domain extent is 12 km off-shore and 400 m deep.

to be that of a classic downwelling, *i.e.* a downward flow along the coastal slope being driven by the incoming flow from the interior.

One of the most striking differences between the two cases is the almost complete reversal of fluid motions in the case of the along-shore wind forced case. There is essentially no reversal of any kind in the off-shore case. We note that in the southern hemisphere the Coriolis effect has opposite sign from that in the northern hemisphere, so an easterly wind along the east-west coast of Antarctica ("into the paper" in these simulations) will end up moving fluid to the left, *i.e.* away from the coast in our setup. This is indeed the case for both wind directions up to about 5 days. Nevertheless, in the along-shore case
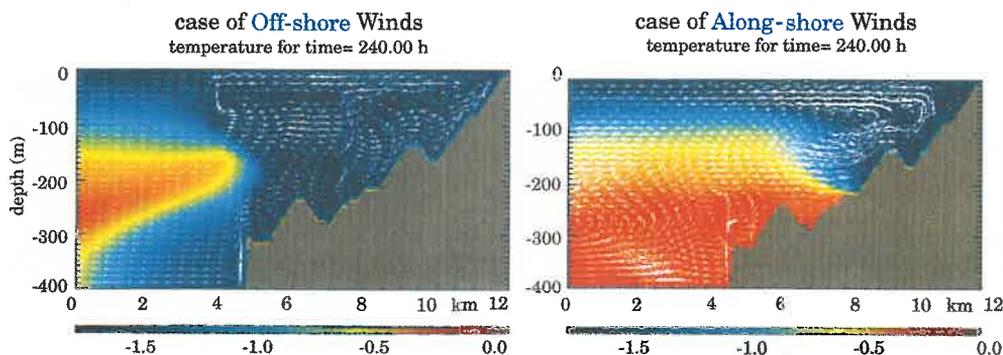
Fig. 4. – High-resolution illustration of the temperature field for the two forcing cases at $t = 10.0$ days. Left figure: off-shore forcing, right figure: along-shore forcing.

the surface flow reverses toward the shore, when the convection plume gets strong and moves closer to shore, and suppresses the upwelling currents.

3'4. *Evolution of the salt field.* – The parallel evolution of the salinity field is illustrated in fig. 5. Since the time evolution of the velocity and temperature fields has been adequately described in the previous figures, we just depict the corresponding salinity fields at three different times: these are sufficient to illustrate the differences between the two cases, and to augment our understanding of what is happening.

Already at $t = 7.5$ days, the off-shore winds have increased drastically the salinity fields above the thermocline region ($< 100\,\mathrm{m}$ depth), and they have done that all the way from the coast to the polynya-edge front; the maximum salinity values in this region, found near the central downwelling plume, are only slightly lower than the original bottom values (maximum at $t = 0$). Interestingly, the frontal downwelling plume has little salinity increase associated with it, and in fact appears to limit the spread of high salinity further off-shore. Note that the descending dense waters along the bottom actually freshen the lower regions (below $200\,\mathrm{m}$), so it is the low temperature caused by the cooling which provides the downward forcing for these motions. By $t = 10$ days the largest salinity values are found between the shore and the central descending plume, clearly indicating where all the brine deposited at the surface is accumulating, at least until this time. The recirculating motions associated with the upwelling and the convective plume are responsible for "trapping" these high salinities near the coast.

In strong contrast, the behavior of the salinity fields in the along-shore case is completely different. There is almost no increase of salinity in the surface layer before day 8, and salt only begins to accumulate near the coast for $t > 10$ days, where apparently the strong downward convective plume is concentrating the deposited brine. Figure 6 illustrates the very slow accumulation of brine-origin salinity in the surface layer. Note that the surface velocities are all toward the shore until they reach a point above the center of the plume, funneling into the plume any deposited brine picked up along the way. Even more interesting is the fact that the flow along the shelf slope is all uphill until about the $180\,\mathrm{m}$ depth; these uphill moving water masses are gradually entrained into off-shore moving currents, with the flow reversal taking place in the 250–$300\,\mathrm{m}$ depth range. Moreover, these deep upwelling currents are forced not that much by the off-shore wind, rather than by the off-shore movement of the "return" currents that are part of the large convection cell.
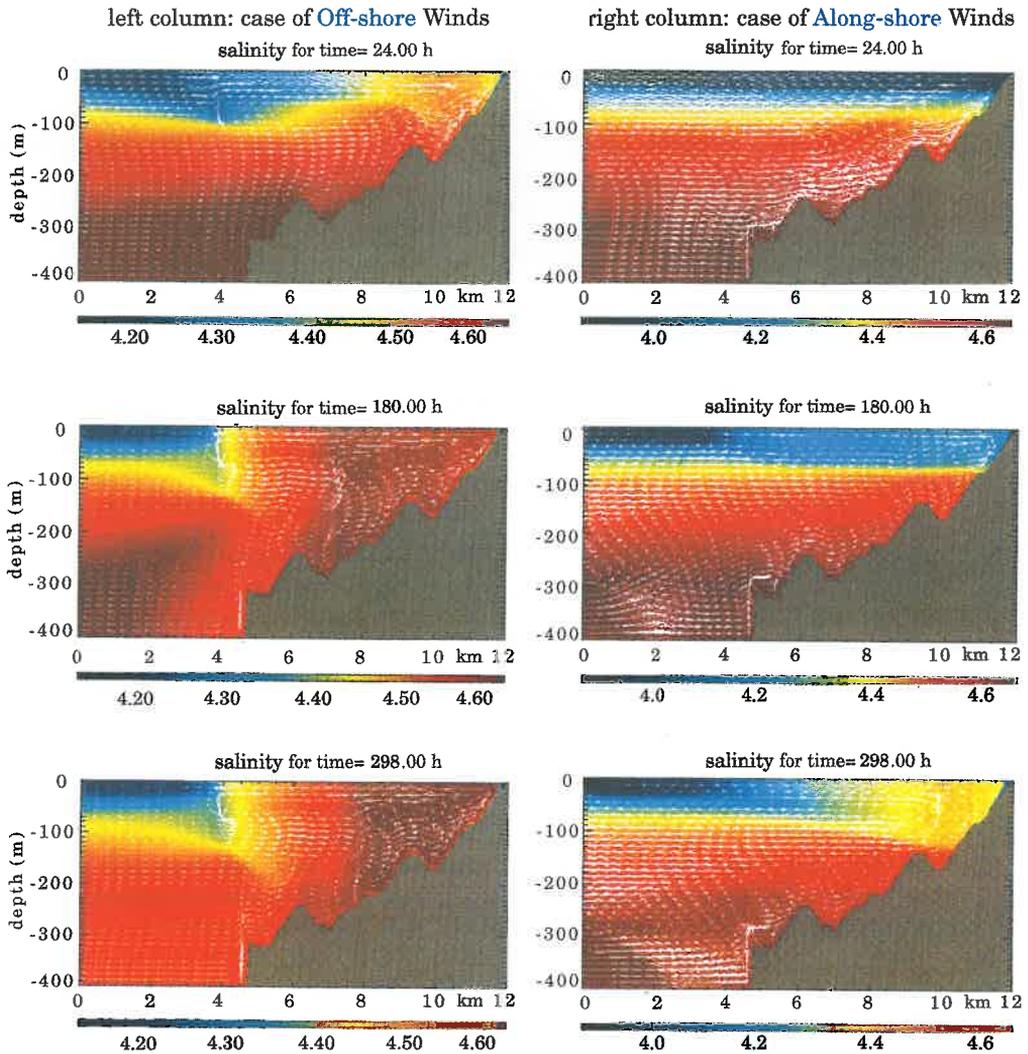
Fig. 5. – Time evolution of the salinity field for the two forcing cases: a) left column, off-shore forcing, b) right column, along-shore forcing. Note that a value of 34.00 has been subtracted from the salinity values to better serve the contouring process.

4. – Summary and conclusions

We have examined the upwelling and convective motions, in a 2.5-D framework including rotation, for wind- and brine-driven forcing under a polynya off the Adelie Coast of Antarctica. In particular, we have examined the differences resulting from off-shore and along-shore wind forcings. These differences were found to be quite important for the production of deep and bottom waters on Antarctic shelves:

a) only off-shore winds produced the formation of a front near the open ocean edge of the polynya, in addition to a second convective plume region closer to shore;
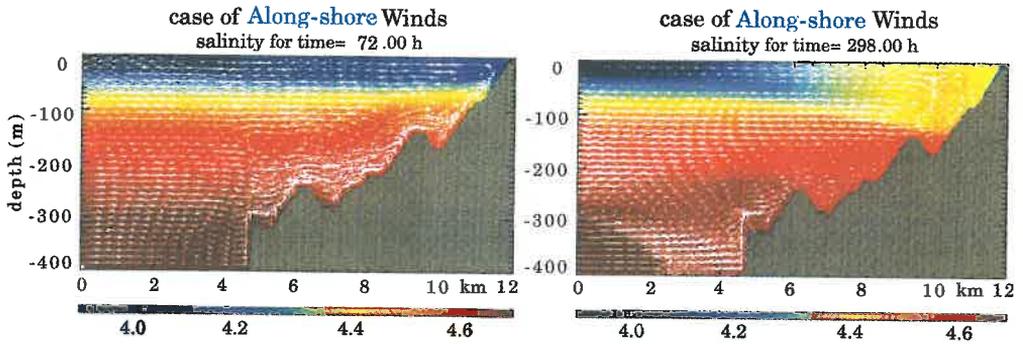
Fig. 6. – High-resolution illustration of the salinity field for the along-shore forcing case. Left figure: $t = 3$ days, right figure: $t = 12.5$ days. As in fig. 5, a value of 34.00 was subtracted from the salinity values.

b) in the off-shore case, the upwelling motions never ceased during the development of strong convective activity, whereas in the along-shore case there was a periodic suppression of the upwelling motions when the convective plumes move close to shore;

c) the onset time and depth of penetration of the dense water plumes moving downs-lope along the bottom was quite different for the two cases: 2 days and 400 m for the off-shore case, and 8 days and 200 m for the along-shore forcing case, respectively;

d) the region above the thermocline (< 100 m depth) is filled with high salinity values, starting at day 2 and extending from the front to the shore, for the off-shore case; whereas the salinity in this region barely reaches the mid-thermocline value at day 12.5 and extends only ~ 3 km from shore, for the along-shore case;

e) the formation of deep upwelling currents along the slope between 400 and 200 meters only for along-shore winds, and the development of strong downward flows of dense water in the same region in the case of off-shore wind forcing.

We conclude that off-shore winds are much more efficient than along-shore winds in producing dense waters on the Antarctic shelves: even intermittent katabatic winds will play a strong role in the formation of water masses that descend into the deep basin to eventually form Antarctic Bottom Water (AABW) in the world ocean.

* * *

REFERENCES

[1] BROECKER W. S., *Oceanog.*, **4** (1991) 79.
[2] BROECKER W. S., *Science*, **278** (1997) 1582.
[3] BINDOFF N. L., WARNER M. J. and NICL S., *International WOCE Newsletter*, **26** (1997) 36.
[4] FOSTER T. D. and CARMACK E. C., *Deep Sea Res.*, **23** (1976) 301.
[5] GAWARKIEWICZ G. and CHAPMAN D. C., *J. Geophys. Res.*, **100** (1995) 4489.
[6] GOLDSTEIN D., HANDLER R. and SIROVICH L., *J. Comp. Phys.*, **105** (1993) 354.
[7] GOLDSTEIN D., HANDLER R. and SIROVICH L., *J. Fluid Mech.*, **302** (1995) 333.
[8] JACOBS S., *Mar. Geol.*, **85** (1989) 121.
[9] JACOBS S. and COMISO J., *J. Geophys. Res.*, **94** (1989) 18195.
[10] JONES H. and MARSHALL J., *J. Phys. Oceanog.*, **23** (1993) 1009.
[11] KAMPF J. and BACKHAUS J. O., *J. Geophys. Res.*, **103** (1998) 5577.
[12] KANTHA L. H. and CLAYSON C. A., *J. Geophys. Res.*, **99** (1994) 25235.
[13] KILLWORTH P., *Rev. Geophys. Space Phys.*, **21** (1983) 1.
[14] MARSHALL J. and SCHOTT F., *Open-ocean convection: observations, theory and models*, Center of Global Change Science Report #52, MIT, Cambridge, MA, USA, 1998.
[15] MELLOR G. L. and YAMADA T., *Rev. Geophys.*, **20** (1982) 851.
[16] MUENCH R. D., SMITH D. C. IV and PAULSON C. A., *J. Geophys. Res.*, **100** (1995) 4681.
[17] PEASE C. H., *J. Geophys. Res.*, **92** (1987) 7049.
[18] PIACSEK S., ALLARD R. and WARN-VARNAS A., *Dynamics Atmos. Oceans*, **27** (1997) 601.
[19] PIACSEK S. and TOOMRE J., *Nonlinear evolution and structure of salt fingers, Marine Turbulence*, edited by J. NIHOUL (Elsevier Press) 1980, p. 193.
[20] POTTS M. A., *A study of convective processes in ice covered seas over topography using a nonhydrostatic model*, Ph.D. Thesis, University of Colorado (1998).
[21] RINTOUL S. R., *On the Origin and Influence of the Antarctic Bottom Water of the southeast Indian Ocean, Oceanology of the Antarctic Continental Margin*, edited by S. JACOBS, *Antarc. Res. Ser.* (American Geophysical Union) 1997.
[22] RUDELS B. and QUADFASEL D., *J. Marine Systems*, **2** (1991) 435.
[23] SCHOTT F., VISBECK M. and FISCHER J., *J. Geophys. Res.*, **98** (1993) 14401.
[24] SCHLOSSER P., BONISCH G., REIN M. and BAYER P., *Science*, **251** (1991) 1054.
[25] SCHNEIDER W. and BUDEUS G., *J. Geophys. Res.*, **100** (1995) 4287.
[26] SMITH S. D., MUENCH R. D. and PEASE C. H., *J. Geophys. Res.*, **95** (1990) 9461.
[27] SMITH D. C. IV and MORISON J. H., *J. Geophys. Res.*, **103** (1998) 3233.
[28] WASHINGTON W. M. and MEEHL G. A., *J. Geophys. Res.*, **101** (1996) 12795.